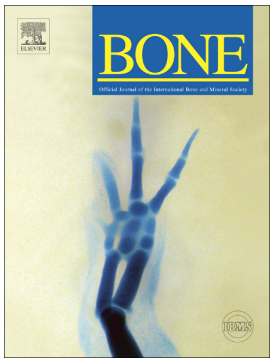

Musculoskeletal phenotype in two unrelated individuals with a recurrent nonsense variant in SGMS2

Marie-Eve Robinson, Ghalib Bardai, Louis-Nicolas Veilleux, Francis H. Glorieux, Frank Rauch

PII: S8756-3282(20)30041-7

DOI: https://doi.org/10.1016/j.bone.2020.115261

Reference: BON 115261

To appear in: *Bone*

Received date: 15 November 2019

Revised date: 22 January 2020

Accepted date: 3 February 2020

Please cite this article as: M.-E. Robinson, G. Bardai, L.-N. Veilleux, et al., Musculoskeletal phenotype in two unrelated individuals with a recurrent nonsense variant in SGMS2, *Bone*(2020), https://doi.org/10.1016/j.bone.2020.115261

Musculoskeletal phenotype in two unrelated individuals with a recurrent nonsense variant in *SGMS2*

Marie-Eve Robinson[1,2], Ghalib Bardai[1], Louis-Nicolas Veilleux[1], Francis H. Glorieux[1], Frank Rauch[1]

1. Shriners Hospital for Children - Canada, McGill University, Montreal, QC, Canada
2. Children's Hospital of Eastern Ontario Research Institute, University of Ottawa, ON, Canada

This study was supported by the Shriners of North America.

Corresponding author: Marie-Eve Robinson, Children's Hospital of Eastern Ontario Research Institute, 401 Smyth Road, Ottawa, Ontario, Canada K1H 8L1; E-mail: mrobinson@cheo.on.ca

Disclosures

The authors state that they have the following disclosures:

Marie-Eve Robinson: None

Ghalib Bardai: None

Louis-Nicolas Veilleux: None

Francis H. Glorieux: Novartis, Amgen and Mereo Biopharma: consulting fees and research grants.

Frank Rauch: Novartis and Mereo BioPharma: consulting fees. Ultragenyx, Catabasis, PreciThera: study grant to institution

Abstract:

Heterozygous mutations in the gene encoding the sphingomyelin synthase 2, *SGMS2*, has recently been linked to childhood-onset osteoporosis and skeletal dysplasia. One nonsense variant at position c.148C>T (p.Arg50*) has been associated with mild bone fragility with or without cranial sclerosis. Here we assessed the effect of the *SGMS2* p.Arg50* variant in two unrelated probands with childhood-onset osteoporosis and their unaffected family members. We found that the p.Arg50* variant was associated with phenotypic variability, ranging from absence of a bone phenotype to severe vertebral compression fractures and low lumbar spine areal bone mineral density (BMD) as measured by dual energy x-ray absorptiometry. Peripheral quantitative computed tomography of the radius and tibia in the two probands revealed low cortical volumetric BMD and reduced cortical thickness. In addition, both probands were obese and suffered from muscle function deficits compared to sex- and age-matched controls. Long-term bisphosphonate treatment was associated with reshaping of previously compressed vertebral bodies.

Key words: Bisphosphonates; Dual-energy X-ray absorptiometry; Peripheral quantitative computed tomography; Osteogenesis imperfecta; *SGMS2*

Introduction

Monogenic bone fragility disorders are caused by genetic variants that can be inherited in an autosomal dominant, autosomal recessive or X-linked fashion. (1) The most common cause of monogenic bone fragility disorders are pathogenic variants affecting the genes encoding collagen type I (*COL1A1* and *COL1A2*). (2) Recently, heterozygous mutations in *SGMS2*, the gene encoding sphingomyelin synthase 2 (SMS2), have been linked to childhood-onset osteoporosis and skeletal dysplasia. (3)

Sphingomyelin is one of the major lipids forming the plasma membrane. SMS2 is an enzyme that resides primarily in the plasma membrane, (4) where it synthesizes sphingomyelin from ceramide and phosphatidylcholine, forming diacylglycerol as a by-product. (5) SMS2 may also play a role in mineralization, as the synthesized sphingomyelin can be cleaved by sphingomyelin phosphodiesterase 3 (SMPD3) to generate ceramide and phosphocholine, a possible source of phosphate. (3) Homozygous *SMPD3* knockout mice have severe bone deformities, fractures and abnormal bone mineralization. (6) No bone phenotype has been reported in homozygous *SGMS2* knockout mice, but these studies focussed on energy metabolism, the central nervous system and atherosclerosis rather than skeletal analyses. (4, 7-9) *SGMS2* knockout mice had increased insulin sensitivity and decreased NFkappa B activation in macrophages. (9)

In humans, the available evidence suggests that some heterozygous missense variants in *SGMS2* (NM_001136257) have a dominant negative effect and lead to severe bone fragility and spondylometaphyseal dysplasia, while one recurrent nonsense variant (c.148C>T, p.Arg50*) has been associated with milder bone fragility with or without cranial sclerosis. (3) So far, the heterozygous *SGMS2* p.Arg50* variant has been reported in 10 individuals from four unrelated families. (3) Nine of these 10 individuals had vertebral fractures, seven had sustained at least one

peripheral fracture, six had mild scoliosis and five individuals had radiographic evidence of sclerotic skull lesions. Short stature (height z-score below -2) was present in three of these individuals. Four individuals had neurological manifestations, in particular transient facial nerve palsies.

The mechanism by which the heterozygous *SGMS2* p.Arg50* variant leads to bone fragility is unclear. No obvious cellular defects were observed in skin fibroblasts. (3) However, it appears that *SGMS2* is most highly expressed in cortical bone, which makes osteoblasts the most interesting cell type for function analyses, but such osteoblast studies have not been reported. Analyses of transiliac bone biopsy samples from two individuals showed that trabecular bone had an increased proportion of poorly mineralized bone and that pyridinoline collagen cross-links were reduced. (3) However, dynamic histomorphometric parameters of bone formation, performed in one individual, showed normal bone formation rate and normal mineralization lag time.

Important aspects of the phenotype associated with the *SGMS2* p.Arg50* variant have not been characterized in detail, such as the impact of the variant on the cortex of long bones and on muscle function. Even though *SGMS2* is most highly expressed in cortical bone, *SGMS2* expression is also found in muscle. (3) SMS2 deficiency could lead to accumulation of its substrate ceramide, which could alter muscle function since ceramide inhibits insulin-stimulated glucose entry into rat myocytes. (10) Regarding medical treatment of bone fragility related to the *SGMS2* p.Arg50* variant, it has been noted that bisphosphonate treatment was associated with decreased peripheral fracture rates in some patients, (3) but the effect of long-term intravenous bisphosphonate therapy on vertebral shape has not been investigated.

In the present study, we evaluated the muscle function, cortical and trabecular bone properties as well as the extraskeletal phenotype of two unrelated individuals with childhood-onset osteoporosis associated with the *SGMS2* p.Arg50* variant. Further, we assessed the skeletal effect of long-term intravenous bisphosphonate therapy in these individuals.

Patients and methods

Subjects

Two patients with the heterozygous *SGMS2* p.Arg50* variant were evaluated at the Shriners Hospital for Children in Montreal and were followed for medical, surgical and rehabilitative care. Their clinical data were extracted by retrospective chart review. Family members harbouring the *SGMS2* pathogenic variant were assessed clinically on one occasion.

The study was approved by the Institutional Review Board of McGill University. All affected family members or their legal guardians provided written informed consent. Assent was provided by participants aged 7 to 17 years.

Bisphosphonate Treatment

Up to the year 2003, individuals with childhood-onset osteoporosis were treated with intravenous pamidronate because of vertebral compression fractures. Pamidronate, administered at an initial annual does of 9 mg per kg of body weight was administered over a 4-hour period on three successive days. (11) In the subsequent years, intravenous zoledronic acid, administered at an initial annual dose of 0.1 mg per kg of body weight, was administered over 45 minutes, the dosing and timing being adjusted based on lumbar spine areal BMD, as previously described. (12) Bisphosphonates were discontinued at achievement of final height. (13)

Clinical assessment

Height was measured using a Harpenden stadiometer (Holtain Limited, Crymych, UK) and weight was determined using mechanical scales (Healthometer, Bridgeview, USA). Height and weight were converted to age- and sex-specific z-scores according to the reference data published by the Centers for Disease Control and Prevention. (14)

Blood and second void urine samples were obtained in the morning after an overnight fast. Alkaline phosphatase, total calcium, phosphorus and urine creatinine concentration was quantified colorimetrically. 25-hydroxyvitamin D was measured by immunochemiluminescence assays on an IDS-iSYS automated analyzer (Immunodiagnostics Systems Limited, UK). Urinary cross-linked N-telopeptides of type I collagen (NTX), a bone resorption marker, was quantified by enzyme-linked immunosorbent assay (ELISA) (Osteomark; Ostex International Inc., Seattle, WA). Urinary NTX/creatinine ratio was expressed as a percentage of age-specific mean reference values using published reference data. (15) Serum leptin was quantified by enzyme immunoassay and compared to reference ranges based on body mass index, gender and development stages, using published reference data. (16) Adiponectin was measured via ELISA, using reference ranges of a commercial laboratory (Mayo Clinic Laboratories, US). Ceramide levels were quantified via liquid chromatography-tandem mass spectrometry, using reference ranges of a commercial laboratory (Mayo Clinic Laboratories, US).

Dual-energy X-ray absorptiometry

Dual-energy X-ray absorptiometry (DXA) was performed in the antero–posterior direction at the lumbar spine (L1–L4) and head using a Hologic QDR Discovery device (Hologic Inc., Waltham,

MA, USA). Lumbar spine areal BMD results and head bone mineral content results were transformed to age- and gender-specific z-scores using published reference data. (17-19)

Spine radiographs

Lateral spine radiographs were evaluated for the presence of vertebral compression fractures using the Genant semiquantitative method from T4 to L4. (20) The vertebral bodies were assigned a severity score: grade 0 (normal), grade 1 (mild), grade 2 (moderate), or grade 3 (severe); and the spinal deformity index (SDI) was calculated by summing up the grade of each vertebra in each patient. (21) Among children with a nonsense *SGMS2* pathogenic variant and vertebral compression fractures, lateral spine radiographs were evaluated multiple times during follow-up to assess for reshaping of previously compressed vertebral bodies. Family members harboring the same *SGMS2* pathogenic variant underwent a lateral spine radiograph on one occasion.

Peripheral quantitative computed tomography

Peripheral quantitative computed tomography (pQCT) was performed at the radius and tibia using the Stratec XCT2000® equipment (Stratec Inc, Pforzheim, Germany) and the manufacturer's software package (version CXT 6.00B). At the radius, measurements were taken at sites corresponding to 4% and 65% of the forearm length. At the tibia, measurements were taken at sites corresponding to 4%, 38% and 66% of the tibia length. A tomographic slice of 2.0 mm thickness was taken at a voxel size of 0.4 x 0.4 x 2 mm. Bone and muscle were separated from fat using a density threshold of 40 mg/cm^3. Muscle was additionally separated from bone using a density threshold of 280 mg/cm^3. A default threshold of 280 mg/cm^3 was used to detect

the outer bone contour at the metaphysis, while a threshold of 710 mg/cm^3 was used at the diaphysis (default equipment setting). The muscle cross-sectional area (expressed as mm^2) was calculated by subtracting the bone cross-sectional area from the combined muscle and bone cross-sectional area. Radius pQCT analyses were transformed to age- and gender-specific z-scores using our published reference data. (22, 23) Tibia pQCT analyses were transformed to age- and gender-specific z-scores using unpublished reference data from our laboratory.

Histomorphometry

A trans-iliac biopsy specimen was obtained in Individual 1 at a site 2 cm posterior and inferior to the superior anterior iliac spine, using a Bordier trephine (5 mm core diameter). Tetracycline double labeling was performed prior to the biopsy. The sections were deplastified with ethylene glycol monoethyl acetate, and later either stained with Goldner trichrome or mounted unstained for fluorescence microscopy. Analysis of the external cortex was performed, and the following primary measures were obtained: external cortical width, cortical bone area, cortical tissue area, bone perimeter, osteoblast perimeter, osteoid area, osteoid perimeter, double label perimeter, interlabel distance, single label perimeter, osteoclast number, osteoclast perimeter and eroded perimeter. With the exception of cortical width, all analyses were performed at a magnification of x200. 3D parameters were derived using the primary measures using standard formulae. (24) Results were compared to reference established in our laboratory. (24)

Characterization of variants

Pathogenic variants in *SGMS2* were identified through whole exome sequencing and were confirmed by Sanger sequencing. Genomic DNA was isolated using the QIAamp DNA mini kit

(Qiagen, Hilden, Germany) from the buffy coat of whole blood. Whole exome sequencing was performed at the McGill University and Génome Québec Innovation Centre (Montreal, Canada). In brief, libraries were generated using the SureSelect*XT* low input Automated Target Enrichment for Illumina Paired-End Multiplexed Sequencing (Agilent, Santa Clara, CA, USA) and using SureSelect Human All Exon V5 (Individual 1) and V6 (Individual 2) enrichment baits as per the manufacturer's recommendations. The captured and amplified libraries were normalized, pooled and loaded at 200pM on an Illumina HiSeq 4000 (Illumina, San Diego, CA, USA) for 2 x 100 cycles (paired-end mode). A phiX library was used as a control and mixed with libraries at 1% level. The program bcl2fastq2 v2.20 was then used to demultiplex samples and generate fastq reads which were imported and analyzed in Illumina's BaseSpace Sequence Hub (Illumina, San Diego, CA, USA) using Enrichment App v3.0. Alignment was performed against the UCSC hg19 pseudoautosomal regions-masked build using the Issac tool (iSAAC-03.16.02.20). Ninety-five percent of bases were covered by ≥ 10 reads.

Muscle function

To assess upper limbs muscle strength, a grip strength dynamometer (Jamar Smart Digital Hand Dynamometer, Jamar Technology Inc., USA) was used. The study participants performed three repetitions with each hand, which were tested in alternance. The maximal grip force in kilograms was retained and transformed to age- and gender-specific z-scores using published reference data. (25)

To assess dynamic lower limbs muscle function, jumping mechanography was used (Leonardo Mechanograph® Ground Reaction Force Plate; Novotec Medical Inc, Pforzheim, Germany). Two tests were performed: (1) A multiple two-legged hopping (M2LH) and (2) a single two-

legged jump (S2LJ), as previously described by our laboratory. (26) Maximal force relative to body weight and maximal power relative to body mass were expressed as a percentage of the expected mean for age and sex using controls from our laboratory.

Functional exercise capacity

A six-minute walk test (*6MWT*) was performed to measure functional exercise capacity. The *6MWT* is a sub-maximal clinical test validated for multiple adult and pediatric populations. (27-29) Individuals covered as much distance as possible by going back and forth along a 20-metre course during a period of six minutes. Patients were instructed to walk at their own self-selected speed and could rest when needed. The distance walked during the six minutes were compared to reference values for adults (30) and children (31) to obtain a predicted distance. A percent deconditioning score was also computed [(walked distance - predicted distance / predicted distance) x100].

Results

Individual 1

Individual 1 is a female born from non-consanguineous parents of French-Canadian descent. She was first presented at our institution at 5.0 years of age for severe back pain. Height was 100.2 cm (z-score -1.6), weight 13.6 kg (z-score -2.3) and body mass index (BMI) 13.5 kg/m^2 (z-score -1.6). The girl had white sclera, normal dentition and normal joint mobility. Spine radiographs showed multiple vertebral compression fractures (Figure 1) and low lumbar spine areal BMD (z-score -4.1). Serum alkaline phosphatase was slightly elevated (39% above the upper limit of the

reference range), while serum levels of 25-hydroxyvitamin D, total calcium, phosphorus and urinary NTX/creatinine (128% of mean) were within the reference range.

A trans-iliac bone biopsy was performed and yielded an incomplete specimen, containing only the external cortex (Figure 3). Histomorphometric analysis revealed high cortical porosity, normal osteoid parameters, normal appearance of tetracycline labels, a slightly diminished mineral apposition rate and a slightly increased mineralization lag time (Table 1). Treatment with intravenous pamidronate was started after this initial evaluation and was associated with complete resolution of back pain. The girl did not have any long-bone fracture, either before or after the start of bisphosphonate treatment.

At six years of age, Individual 1 started to experience migraines with aura in the setting of an otherwise normal neurological examination. By 9 years of age, she had mild scoliosis as well as mild genu valgum secondary to tibia bowing (Figure 1). After 11 years of intravenous bisphosphonate treatment (pamidronate for the first 4 years, zoledronate thereafter), lumbar spine areal BMD z-score had increased to -1.7. Previously compressed vertebrae had undergone significant reshaping (Figure 1).

Whole exome sequencing revealed a c.148C>T variant in *SGMS2* introducing a premature stop codon in exon 2 (p.Arg50*). The variant was confirmed by Sanger sequencing (Figure 1). Sanger sequencing failed to detect the variant in either of the parents, which were both healthy and non-obese. Thus, the p.Arg50* variant seemed to have arisen de novo in Individual 1.

At the age of 16 years 5 months, the girl had a normal height (154 cm; z-score -1.4) and a normal weight (53.2 kg; z-score -0.2; BMI 22.4 kg/m^2; z-score +0.5). At the time of the last evaluation at 22 years of age, Individual 1 had a normal height (156 cm, z-score -1.2) and was obese (weight 89.2 kg, z-score +1.9; BMI 36.7 kg/m^2, z-score + 2.0), which could not be attributed to clear

lifestyle factors. Serum concentrations of fasting insulin, glucose, HbA1C, cholesterol, free fatty acids, leptin, adiponectin and ceramide were within normal limits. Lumbar spine areal BMD z-score was -1.5. Bone mineral content of the head was 250 g (z-score -2.8). Radius and tibia pQCT showed normal trabecular volumetric BMD, but low cortical volumetric BMD and low cortical thickness (Table 2 and Figure 1). Her calf muscle cross-sectional area was normal (Table 2). Grip force was at the lower limit of the reference range, while mechanography results were lower than in healthy individuals of the same age and sex (Table 3). After adjusting for her height and weight, distances walked during the *6MWT* test were lower than healthy adults (Table 3).

Individual 2

Individual 2 is a male born from non-consanguineous parents of French, Swedish, English and French-Canadian descent. He was first evaluated at our institution at 8.7 years of age for a history of two low-trauma long-bone fractures (first fracture at the age of 4 years) and severe back pain. He also had a history of brief episodes of unresponsiveness of unclear etiology as well as intermittent bowel incontinence. Electroencephalogram, brain and spine magnetic resonance imaging were normal. He had normal stature (height 128 cm, z-score -0.7) and was overweight (weight 36.7 kg, z-score +1.4; BMI 22.4 kg/m^2, z-score +1.9). Joints had normal mobility and sclera were white. Teeth appeared normal in shape and color, but he had dental crowding (Figure 2) and a history of delayed primary tooth eruption (first tooth eruption: 19 months, normal range: 6-10 months old). (32)

Radiographs showed multiple vertebral compression fractures, mild scoliosis, normal skull and mild genu valgum secondary to tibia bowing (Figure 2). Lumbar spine areal BMD was low (z-

score -3.1). Radius pQCT revealed low trabecular and cortical volumetric BMD and low cortical thickness (Table 2 and Figure 2). Serum alkaline phosphatase, serum 25-hydroxyvitamin D, total serum calcium and serum phosphorus levels were normal. Treatment with intravenous zoledronate was started after the initial evaluation and was continued until the time of the last follow up. Bisphosphonate therapy was associated with complete resolution of back pain. He did not sustain any more long-bone fractures after the start of zoledronate treatment.

Whole exome sequencing in DNA from Individual 2 and his parents revealed the *SGMS2* p.Arg50* variant in both the boy and his father (Figure 2). Neither the chromatogram (Figure 2) nor the whole exome sequencing data suggested mosaicism for the *SGMS2* p.Arg50* variant in the DNA extracted from whole blood of the father. Out of 110 reads obtained at position c.148, 50 reads showed the *SGMS2* p.Arg50* variant (45%). In addition to the *SGMS2* variant, Individual 1 and his father had a variant of unknown significance in *COL1A1* (c.4351G>T, p.Asp1451Tyr). The father was 40 years of age and had a history of chronic back pain and cardiac arrhythmia but did not have a history of a low-trauma long-bone fracture. He had normal height (177.8 cm) and suffered from obesity (weight 122 kg; BMI 38.6 kg/m^2). The unaffected mother also suffered from obesity (height 156.1cm; weight 95.8kg; BMI 39.3 kg/m^2). Lumbar spine areal BMD in the father was normal (z-score -0.6) and lateral spine radiographs revealed absence of vertebral compression fractures.

Individual 2 was last evaluated at 12.2 years of age. He had delayed loss of primary teeth (first tooth loss at 12 years old; normal range: 6-7 years old). He had normal height (156 cm, z-score +0.8), and was obese (80.4 kg, z-score +2.6; BMI 33.0 kg/m^2, z-score +2.4) but had normal fasting insulin, glucose, HbA1C, cholesterol, free fatty acids, leptin, adiponectin and normal serum ceramide levels. Lumbar spine areal BMD z-score had increased to -1.3. Bone mineral

content of the head was 193 g (z-score -2.9). Previously compressed vertebrae had undergone partial reshaping (Figure 2). On radius and tibia pQCT, trabecular volumetric BMD was normal, while cortical volumetric BMD remained low (Table 2). Calf muscle cross-sectional areal was normal (Table 2). Grip force was at the lower limit of the reference range, while mechanography results and distances walked during the *6MWT* test were lower than healthy individuals of the same age and sex (Table 3).

Discussion

In this study, we found that individuals with the p.Arg50* variant in *SGMS2* seem to present with phenotypic variability, ranging from absence of a bone phenotype to severe vertebral compression fractures and low BMD resembling OI. Among individuals with *SGMS2*-associated osteoporosis, we observed strikingly low cortical volumetric BMD and cortical thickness at the radial and tibial shaft. Intravenous bisphosphonate treatment was associated with a significant increase in BMD at the lumbar spine and distal radius as well as reshaping of previously compressed vertebral bodies.

The absence of a bone phenotype despite the presence of the p.Arg50* variant in the father of Individual 2 indicates variable penetrance. To date, all 10 individuals previously reported with the p.Arg50* variant had an osteoporotic phenotype (Table 4). (3) Although not reported with the *SGMS2* gene, nonsense mutations with incomplete penetrance have been reported with other genetic variants. (33) While the mechanism of the variable penetrance of *SGMS2*-associated osteoporosis is unknown, other modifier genes or increased compensation of the normal *SGMS2* allele may be at play.

The mechanism involved in *SGMS2*-associated osteoporosis is unknown. The severely low cortical volumetric BMD at the tibia and radius that we observed in the presented individuals may reflect the high cortical porosity, as indicated by our histomorphometric results. Although the osteoid surface per bone surface and mineralizing surface per bone surface were minimally elevated in the bone sample of Individual 1, we did not find clear evidence of a mineralization defect, as osteoid thickness was normal, and tetracycline labels were not blurred (Figure 3). However, mineral apposition rate was low, suggesting an osteoblast defect. Previous quantitative backscattered electron imaging of trans-iliac cortical bone in two individuals with the p.Arg50* variant yielded discrepant results in regard to the presence or absence of a mineralization defect. (3)

Pekkinen and colleagues had postulated that the disturbance and mesh-like appearance of the bone matrix (typically observed in primary bone) in histomorphometric studies of individuals with the p.Arg50* variant could contribute to the observed low bone strength. (3) However, bone lamellae were well organized in the bone biopsy of Individual 1 in the present study. Although the mechanism by which decreased plasma membrane sphingomyelin activity leads to low BMD remains unclear, the fact that cortical bone is more severely affected than trabecular bone in our patients aligns with the abundant *SGMS2* mRNA expression in mouse cortical bone. (3)

Individuals with the p.Arg50* variant had a bisphosphonate response that appeared similar to what is observed in individuals with OI caused by *COL1A1/COL1A2* pathogenic variants. (12) We have previously reported that lumbar spine areal BMD increased by 2.6 standard deviations in the first four years of pamidronate therapy in OI type I, III or IV, (34) which is comparable to the observed 2.1 standard deviation increase in individuals with the p.Arg50* variant. In fact, both lumbar spine areal BMD and distal radius volumetric BMD normalized with

bisphosphonate treatment in the present study. The bisphosphonate-mediated vertebral body reshaping described in our study was also previously noted in individuals with moderate to severe OI caused by *COL1A1/COL1A2* mutations. (35) Pekkinen and colleagues found that osteoclasts had normal formation and function in peripheral blood monocytes from patients with the p.Arg50* variant. (3) The good bisphosphonate response that we observed suggests a good availability of osteoclasts.

The dental crowding found in Individual 2 could be secondary to the reported delayed loss of secondary teeth and/or small maxillary bone. Dental abnormalities have not been observed so far in individuals with *SGMS2* pathogenic variants. (3) In addition, sclerotic skull lesions have been described in individuals with *SGMS2* pathogenic variants, (3) but we surprisingly found low skull bone mineral content in both Individual 1 and 2. Further characterization of the craniofacial features of individuals with *SGMS2* pathogenic variants is needed.

The observed normal grip strength might have been influenced by previous bisphosphonate treatment, as isometric grip force improves with bisphosphonate treatment in children and adolescents with OI. (36, 37) On the other hand, we found a deficit in muscle force and power and in the *6MWT* in Individuals 1 and 2 in the presence of normal muscle cross-sectional area and normal ligament laxity. While mRNA expression of *SGMS2* is very low in mouse muscle, (3) the inhibitory effect of the substrate ceramide on insulin-stimulated glucose uptake in skeletal muscle (10) might explain our findings, as ceramide should theoretically be elevated in the setting of SMS2 deficiency. However, it is likely that the muscle function deficits that we found were exacerbated by obesity or low levels of physical activity.

The obesity in Individuals 1 and 2 contrast with the protective effect of SMS2 deficiency on high fat diet-induced obesity in SMS2 knockout mice. (4, 7) The low plasma sphingomyelin in those

mice was associated with improved insulin sensitivity, lipid droplet formation and triglyceride accumulation. It is possible that the obesity observed in our patients is secondary to a lack of exercise due to history of fracture, pain or environmental factors, rather than SMS2 deficiency itself.

The present study is limited in that it reports information on only two individuals. Also, the observed bone and muscle phenotype in the two probands are potentially confounded by the presence of obesity. The study also does not provide functional analyses on the effect of the *SGMS2* abnormality on osteoblasts.

In conclusion, our study suggests that the *SGMS2* p.Arg50* variant is associated with bone fragility with incomplete penetrance. Among individuals with *SGMS2*-associated osteoporosis, cortical bone is thin and porous and seems more severely affected than trabecular bone. Intravenous bisphosphonate therapy appears to be effective to increase BMD and reshape previously compressed vertebrae. Additional research should evaluate mRNA expression of *SGMS2* in human cortical bone and muscle. Moreover, further insight on the role of *SGMS2* on osteoblast function is warranted, as this could unveil new pharmacological targets to improve bone formation.

Acknowledgments

This work was supported by the Shriners of North America.

Authors' roles: Study design: MER and FR. Data collection: MER. Contributed patient information: FG and FR. Sequence analysis: GB. Functional exercise capacity and muscle function testing: LNV. Data interpretation: MER and FR. Drafting manuscript: MER. Revising manuscript content and approving final version of manuscript: all authors. MER and FR take responsibility for the integrity of the data analyses.

References

1. Robinson ME, Rauch F. Mendelian bone fragility disorders. Bone. 2019;126:11-7.
2. Bardai G, Moffatt P, Glorieux FH, Rauch F. DNA sequence analysis in 598 individuals with a clinical diagnosis of osteogenesis imperfecta: diagnostic yield and mutation spectrum. Osteoporos Int. 2016;27:3607-13.
3. Pekkinen M, Terhal PA, Botto LD, Henning P, Makitie RE, Roschger P, et al. Osteoporosis and skeletal dysplasia caused by pathogenic variants in SGMS2. JCI Insight. 2019;4.
4. Li Z, Zhang H, Liu J, Liang CP, Li Y, Li Y, et al. Reducing plasma membrane sphingomyelin increases insulin sensitivity. Mol Cell Biol. 2011;31:4205-18.
5. Taniguchi M, Okazaki T. The role of sphingomyelin and sphingomyelin synthases in cell death, proliferation and migration-from cell and animal models to human disorders. Biochim Biophys Acta. 2014;1841:692-703.
6. Aubin I, Adams CP, Opsahl S, Septier D, Bishop CE, Auge N, et al. A deletion in the gene encoding sphingomyelin phosphodiesterase 3 (Smpd3) results in osteogenesis and dentinogenesis imperfecta in the mouse. Nature Genetics. 2005;37:803-5.
7. Mitsutake S, Zama K, Yokota H, Yoshida T, Tanaka M, Mitsui M, et al. Dynamic modification of sphingomyelin in lipid microdomains controls development of obesity, fatty liver, and type 2 diabetes. J Biol Chem. 2011;286:28544-55.
8. Zhang Y, Dong J, Zhu X, Wang W, Yang Q. The effect of sphingomyelin synthase 2 (SMS2) deficiency on the expression of drug transporters in mouse brain. Biochem Pharmacol. 2011;82:287-94.
9. Hailemariam TK, Huan C, Liu J, Li Z, Roman C, Kalbfeisch M, et al. Sphingomyelin synthase 2 deficiency attenuates NFkappaB activation. Arterioscler Thromb Vasc Biol. 2008;28:1519-26.
10. Gorski J, Dobrzyn A, Zendzian-Piotrowska M. The sphingomyelin-signaling pathway in skeletal muscles and its role in regulation of glucose uptake. Ann N Y Acad Sci. 2002;967:236-48.
11. Rauch F, Glorieux FH. Osteogenesis imperfecta. Lancet. 2004;363:1377-85.
12. Trejo P, Rauch F. Osteogenesis imperfecta in children and adolescents-new developments in diagnosis and treatment. Osteoporos Int. 2016;27:3427-37.
13. Robinson ME, Trejo P, Palomo T, Glorieux FH, Rauch F. Osteogenesis Imperfecta: Skeletal Outcomes After Bisphosphonate Discontinuation at Final Height. J Bone Miner Res. 2019;34:2198-204.
14. Ogden CL, Kuczmarski RJ, Flegal KM, Mei Z, Guo S, Wei R, et al. Centers for Disease Control and Prevention 2000 growth charts for the United States: improvements to the 1977 National Center for Health Statistics version. Pediatrics. 2002;109:45-60.
15. Bollen AM, Eyre DR. Bone resorption rates in children monitored by the urinary assay of collagen type I cross-linked peptides. Bone. 1994;15:31-4.
16. Blum W.F KW, Rascher W. "Reference Ranges of Leptin Levels According to Body Mass Index, Gender and Development Stage" in Leptin: The Voice of Adipose Tissue. Barth JA, editor: Mountainview Books, LLC; 1997.
17. Kalkwarf HJ, Zemel BS, Yolton K, Heubi JE. Bone mineral content and density of the lumbar spine of infants and toddlers: influence of age, sex, race, growth, and human milk feeding. J Bone Miner Res. 2013;28:206-12.

18. Zemel BS, Kalkwarf HJ, Gilsanz V, Lappe JM, Oberfield S, Shepherd JA, et al. Revised reference curves for bone mineral content and areal bone mineral density according to age and sex for black and non-black children: results of the bone mineral density in childhood study. J Clin Endocrinol Metab. 2011;96:3160-9.
19. Faulkner RA, Bailey DA, Drinkwater DT, Wilkinson AA, Houston CS, McKay HA. Regional and total body bone mineral content, bone mineral density, and total body tissue composition in children 8-16 years of age. Calcif Tissue Int. 1993;53:7-12.
20. Genant HK, Wu CY, van Kuijk C, Nevitt MC. Vertebral fracture assessment using a semiquantitative technique. J Bone Miner Res. 1993;8:1137-48.
21. Kerkeni S, Kolta S, Fechtenbaum J, Roux C. Spinal deformity index (SDI) is a good predictor of incident vertebral fractures. Osteoporos Int. 2009;20:1547-52.
22. Rauch F, Schoenau E. Peripheral quantitative computed tomography of the proximal radius in young subjects - new reference data and interpretation of results. J Musculoskelet Neuronal Interact. 2008;8:217-26.
23. Rauch F, Schoenau E. Peripheral quantitative computed tomography of the distal radius in young subjects - new reference data and interpretation of results. J Musculoskelet Neuronal Interact. 2005;5:119-26.
24. Rauch F, Travers R, Glorieux FH. Cellular activity on the seven surfaces of iliac bone: a histomorphometric study in children and adolescents. J Bone Miner Res. 2006;21:513-9.
25. Wong SL. Grip strength reference values for Canadians aged 6 to 79: Canadian Health Measures Survey, 2007 to 2013. Health Reports. 2016;27:3-10.
26. Veilleux LN, Rauch F. Reproducibility of jumping mechanography in healthy children and adults. J Musculoskelet Neuronal Interact. 2010;10:256-66.
27. Gulmans VA, van Veldhoven NH, de Meer K, Helders PJ. The six-minute walking test in children with cystic fibrosis: reliability and validity. Pediatr Pulmonol. 1996;22:85-9.
28. Lelieveld OT, Takken T, van der Net J, van Weert E. Validity of the 6-minute walking test in juvenile idiopathic arthritis. Arthritis Rheum. 2005;53:304-7.
29. Morinder G, Mattsson E, Sollander C, Marcus C, Larsson UE. Six-minute walk test in obese children and adolescents: Reproducibility and validity. Physiotherapy Research International. 2009;14:91-104.
30. Burr JF, Bredin SS, Faktor MD, Warburton DE. The 6-minute walk test as a predictor of objectively measured aerobic fitness in healthy working-aged adults. Phys Sportsmed. 2011;39:133-9.
31. Ulrich S, Hildenbrand FF, Treder U, Fischler M, Keusch S, Speich R, et al. Reference values for the 6-minute walk test in healthy children and adolescents in Switzerland. BMC Pulmonary Medicine. 2013;13:49.
32. Lunt RC, Law DB. A review of the chronology of eruption of deciduous teeth. J Am Dent Assoc. 1974;89:872-9.
33. Singh SM, Casey SA, Berg AA, Abdelhadi RH, Katsiyiannis WT, Bennett MK, et al. Autosomal-dominant biventricular arrhythmogenic cardiomyopathy in a large family with a novel in-frame DSP nonsense mutation. Am J Med Genet A. 2018;176:1622-6.
34. Rauch F, Plotkin H, Zeitlin L, Glorieux FH. Bone mass, size, and density in children and adolescents with osteogenesis imperfecta: effect of intravenous pamidronate therapy. J Bone Miner Res. 2003;18:610-4.

35. Palomo T, Fassier F, Ouellet J, Sato A, Montpetit K, Glorieux FH, et al. Intravenous bisphosphonate therapy of young children with osteogenesis imperfecta: skeletal findings during follow up throughout the growing years. J Bone Miner Res. 2015;30:2150-7.
36. Montpetit K, Plotkin H, Rauch F, Bilodeau N, Cloutier S, Rabzel M, et al. Rapid increase in grip force after start of pamidronate therapy in children and adolescents with severe osteogenesis imperfecta. Pediatrics. 2003;111:E601-3.
37. Land C, Rauch F, Montpetit K, Ruck-Gibis J, Glorieux FH. Effect of intravenous pamidronate therapy on functional abilities and level of ambulation in children with osteogenesis imperfecta. J Pediatr. 2006;148:456-60.

Table 1. Results of histomorphometric analyses of the trans-iliac external cortex in Individual 1

	Results	Reference data
Structural parameters		
External cortical width (µm)	762	794 (316)
Cortical porosity (%)	23.1	9.3 (3.3)
Formation parameters		
Osteoblast surface per bone surface (%)	40	23 (9)
Osteoid thickness (µm)	8.8	8.5 (1.1)
Osteoid surface per bone surface (%)	55	37 (10)
Osteoid volume per bone volume (%)	3.4	1.1 (0.5)
Mineralizing surface per bone surface (%)	44	28 (10)
Mineral apposition rate (µm/day)	0.81	1.34 (0.30)
Mineralization lag time (days)	13.5	8.9 (1.5)
Bone formation rate per bone surface ($\mu m^3 * \mu m^{-2} * y^{-1}$)	130	131 (43)
Resorption parameters		
Eroded surface per bone surface (%)	24	34 (14)
Osteoclast surface per bone surface (%)	1.4	2.8 (1.5)
Osteoclast number per bone perimeter (n per mm)	0.72	0.9 (0.5)

Values are mean (SD).

Table 2. Results of peripheral quantitative computed tomography (pQCT) at the forearm and at the lower leg

	Site	Individual 1 After BP	Individual 2 Before BP	Individual 2 After BP
Age (years)		22	8.7	12.2
Radius				
Trabecular vBMD (z-score)	4%	-1.9	-3.8	-1.7
Cortical thickness (z-score)	65%	-4.4	-3.4	-0.7
Cortical vBMD (z-score)	**65%**	**-6.5**	**-4.0**	**-2.9**
Muscle CSA (z-score)	65%	-0.2	+0.2	+1.0
Tibia				
Trabecular vBMD (z-score)	4%	+0.2	-	+1.7
Cortical thickness (z-score)	38%	-4.6	-	+0.4
Cortical vBMD (z-score)	**38%**	**-3.7**	**-**	**-2.6**
Muscle CSA (z-score)	66%	-1.6	-	+0.1

Site refers to the location on the forearm or lower leg where the pQCT scan was performed.

BP, bisphosphonate; CSA, cross-sectional area; N/A, non applicable; vBMD, volumetric bone mineral density

Table 3. Muscle function and six-minute walk test

	Individual 1	Individual 2
Age at the time of the test (years)	22	12
Grip force (z-score)		
Right hand	-0.7	-1.5
Left hand	-0.7	-2.0
6*MWT*		
Distance performed (m)	439	366
Distance predicted (m)	576	679
Deconditioning (%)	-24	-46
Mechanography (% of expected mean for age and sex)		
M2LH (relative force in multiples of body weight)	-28	-51
S2LJ (relative power in W/Kg)	-20	-26

M2LH, multiple two-legged hopping; N/A, not applicable; S2LJ, single two-legged jump

Table 4. Clinical characteristics of individuals with a heterozygous p.Arg50* variant in the *SGMS2* gene

	Back pain	VF	Scoli-osis	Low-trauma Non-VF (n)	Joint hyper-laxity	Dentition	Myo-pia	Neurological symptoms
Present Report								
I-1	++	+	+	1	-	normal	-	Migraines with aura (altered vision, flashes of light)
I-2	++	+	+	3	-	Delayed eruption, loss of primary teeth; dental crowding	+	Episodes of unresponsiveness, bowel incontinence
Father of I-2	+	-	-	0	-	Dental crowding	+	-
Pekkinen et al (3)								
F1-1		+	+	6			-	Migraines, transient FNP, hand tremors, dystonia
F1-2		+	+	>9			-	FNP, episodes of oculomotorius and trochlearis paresis, trigeminus neuralgia, cephalalgia, canalis carpi, clonic Achilles reflex, depression
F1-3		+	+	>14			-	Alzheimer's disease, transient brain ischemic attack, subdural hematomas, transient FNP, temporary oculomotorius paresis, abducens paresis, depression
F2-1		+	+	9			-	-
F3-1		+	+	0			-	
F3-2		+	-	1			-	-
F3-3		+	-	0			-	-
F3-4		+	-	2			-	-
F3-5		-	-	15			-	Migraines, transient FNP
F4-1	+	+	+	6			+	-

I, Individual; N/A, not available; FNP, facial nerve palsy; VF, vertebral fractures

Figure Legends

Figure 1. Characteristics of individual 1. (A) Pedigree of the family of Individual 1 and chromatograph showing the results of Sanger sequencing in Individual 1. Black symbols represent individuals with osteoporosis. Individuals with the *SGMS2* p.Arg50* variant are marked with an asterisk. Individuals with normal BMD and absence of vertebral compression fractures on lateral spine radiographs are marked with an N (normal). Individuals 1 is marked with a P (proband). (B, C) Lateral spine radiographs at the ages of 5.0 years (B) and 20.0 years (C). There are multiple vertebral compression fractures prior to bisphosphonate (BP) treatment. Bisphosphonate treatment was associated with reshaping of vertebral deformities. (D) Mild tibia bowing at 8.0 years of age. (E) Scoliosis at 15.8 years of age, requiring bracing therapy. (F) Cobblestone appearance of the skull at 6.3 years of age. (G) Forearm pQCT scans at the 65% site (diaphysis) of a 23-year-old healthy woman (left image; cortical bone mineral density of the radius: 1157 mg/cm^3; z-score: +0.2; cortical thickness: 2.6 mm; z-score: +0.4) compared to Individual 1 at 22.1 years of age (right image; cortical volumetric bone mineral density of the radius: 973 mg/cm^3; z-score: -6.5; cortical thickness: 1.3 mm; z-score: -4.4).

Figure 2. Characteristics of individual 2. (A) Pedigree of the family of Individual 2 and chromatographs showing the results of Sanger sequencing in Individual 2 and his father. Black symbols represent individuals with osteoporosis. Individuals with the *SGMS2* p.Arg50* variant are marked with an asterisk. Individuals with normal BMD and absence of vertebral compression fractures on lateral spine radiographs are marked with an N (normal). Individuals 2 is marked with a P (proband). (B, C) Lateral spine radiographs at the ages of 8.2 years (B) and 12.2 years (C). There are multiple severe vertebral compression fractures prior to bisphosphonate (BP) treatment. Bisphosphonate treatment was associated with reshaping of vertebral deformities. (D)

Mild tibia bowing at 8.9 years of age. (E) Scoliosis at 12.2 years of age. (F) Panorex at 6.3 years of age, showing dental crowding of all primary teeth requiring extraction of five primary teeth. (G) Panorex of at 12.1 years of age, showing dental crowing of secondary teeth requiring extraction of two secondary teeth. (H) Forearm pQCT scans at the 4% site (metaphysis) of an 8-year-old healthy boy (left image; trabecular volumetric bone mineral density of the radius: 206 mg/cm3; z-score: +0.3) compared to Individual 2 at 8.7 years of age (right image; trabecular volumetric bone mineral density of the radius: 108 mg/cm^3; z-score: -3.8).

Figure 3. Iliac bone sample of Individual 1 at 5.1 years of age compared to a control sample of a 3.6-year-old girl. Only the external cortex could be obtained in Individual 1. (A, B) View of the entire sample. Mineralized bone is stained green, unmineralized osteoid is stained red/orange (Goldner staining). Size bar represents 1 mm. (C, D) Close-up view of the external cortex, showing increased porosity in Individual 1 (asterisks) (Goldner staining, size bar 100 µm). (E, F) View under polarized light showing normal lamellation in both samples (arrows). No Sharpey fibers or woven bone are seen (toluidine blue staining, size bar 100 µm). (G, H) View under fluorescent light. The tetracycline double labels can be clearly distinguished in both samples (arrows) (unstained, size bar 100 µm).

Manuscript title: Musculoskeletal phenotype in two unrelated individuals with a recurrent nonsense variant in *SGMS2*

Highlights*:*

- *SMGS2*-associated osteoporosis resembles osteogenesis imperfecta
- The *SGMS2* p.Arg50* variant is associated with bone fragility with incomplete penetrance
- Cortical bone is thin and porous in *SGMS2*-associated osteoporosis
- Bisphosphonates seem to be effective at treating *SGMS2*-associated osteoporosis

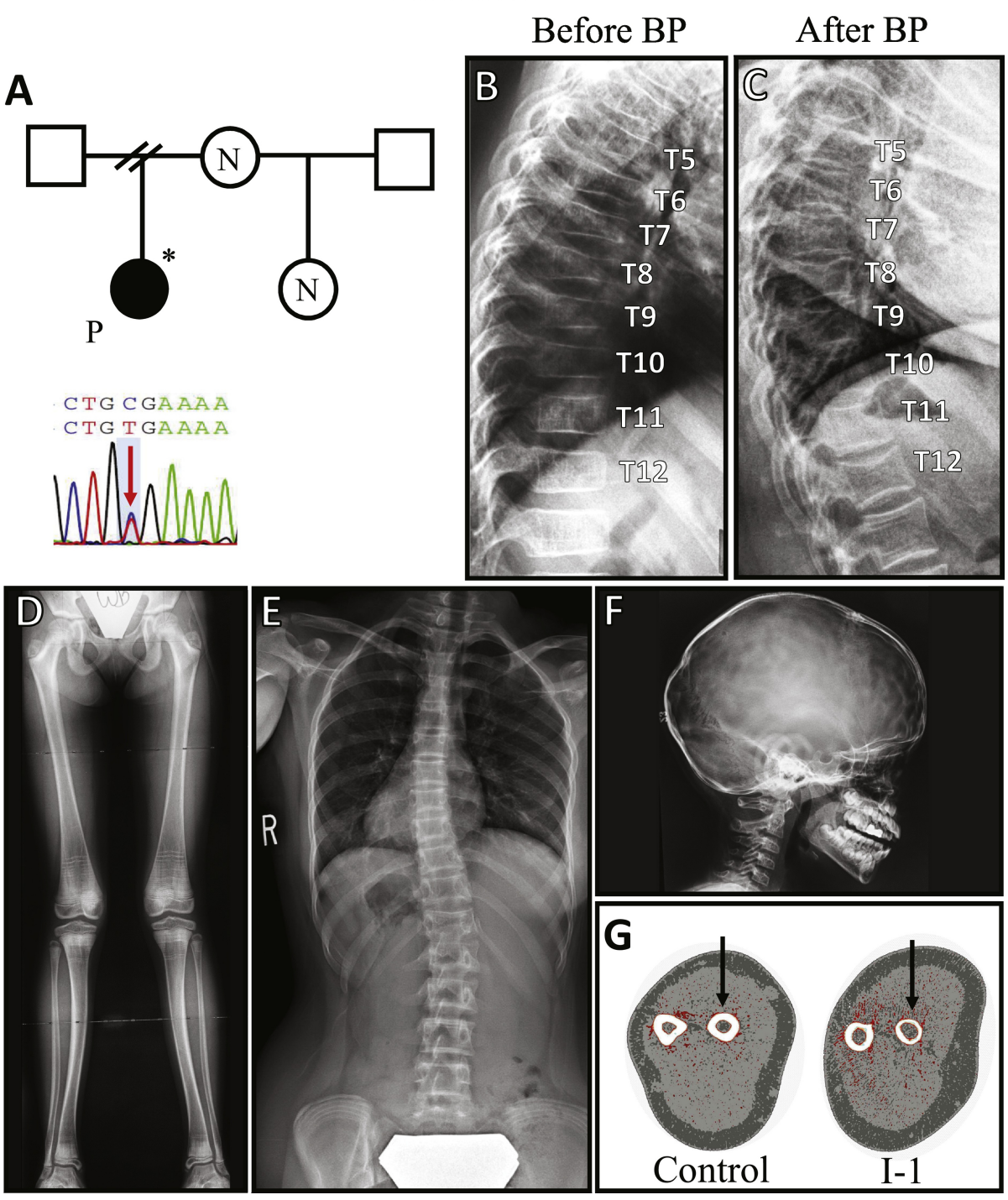
Individual 1
Before BP
After BP
A
N
N
*
P
CTG CGAAAA
CTG TGAAAA
B
T5
T6
T7
T8
T9
T10
T11
T12
C
T5
T6
T7
T8
T9
T10
T11
T12
D
E
R
F
G
Control
I-1

Figure 1

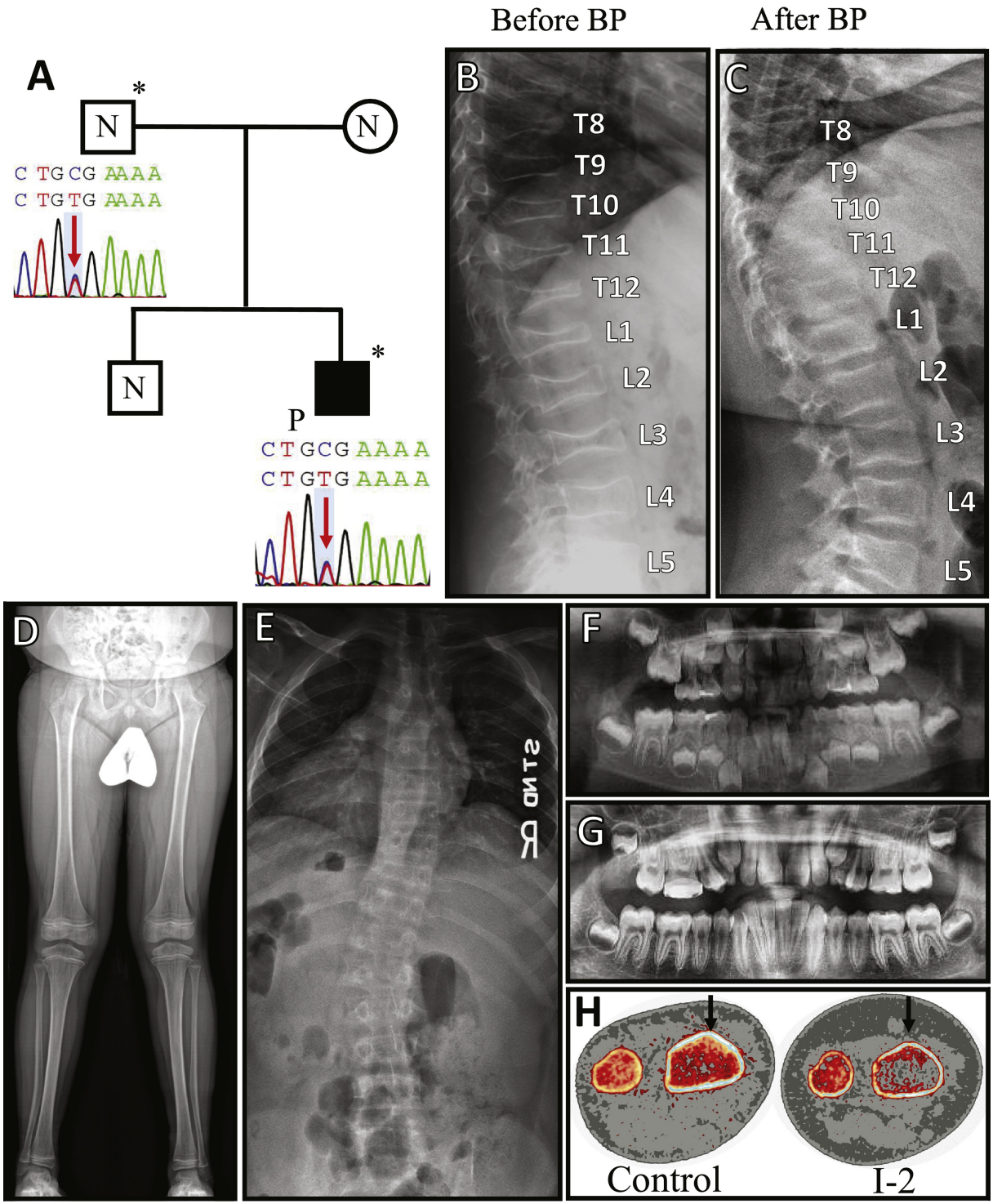
Individual 2
Before BP
After BP
A
N
N
N
P
C T G C G A A A A
C T G T G A A A A
C T G C G A A A A
C T G T G A A A A
B
C
T8
T9
T10
T11
T12
L1
L2
L3
L4
L5
D
E
F
G
H
Control
I-2

Figure 2

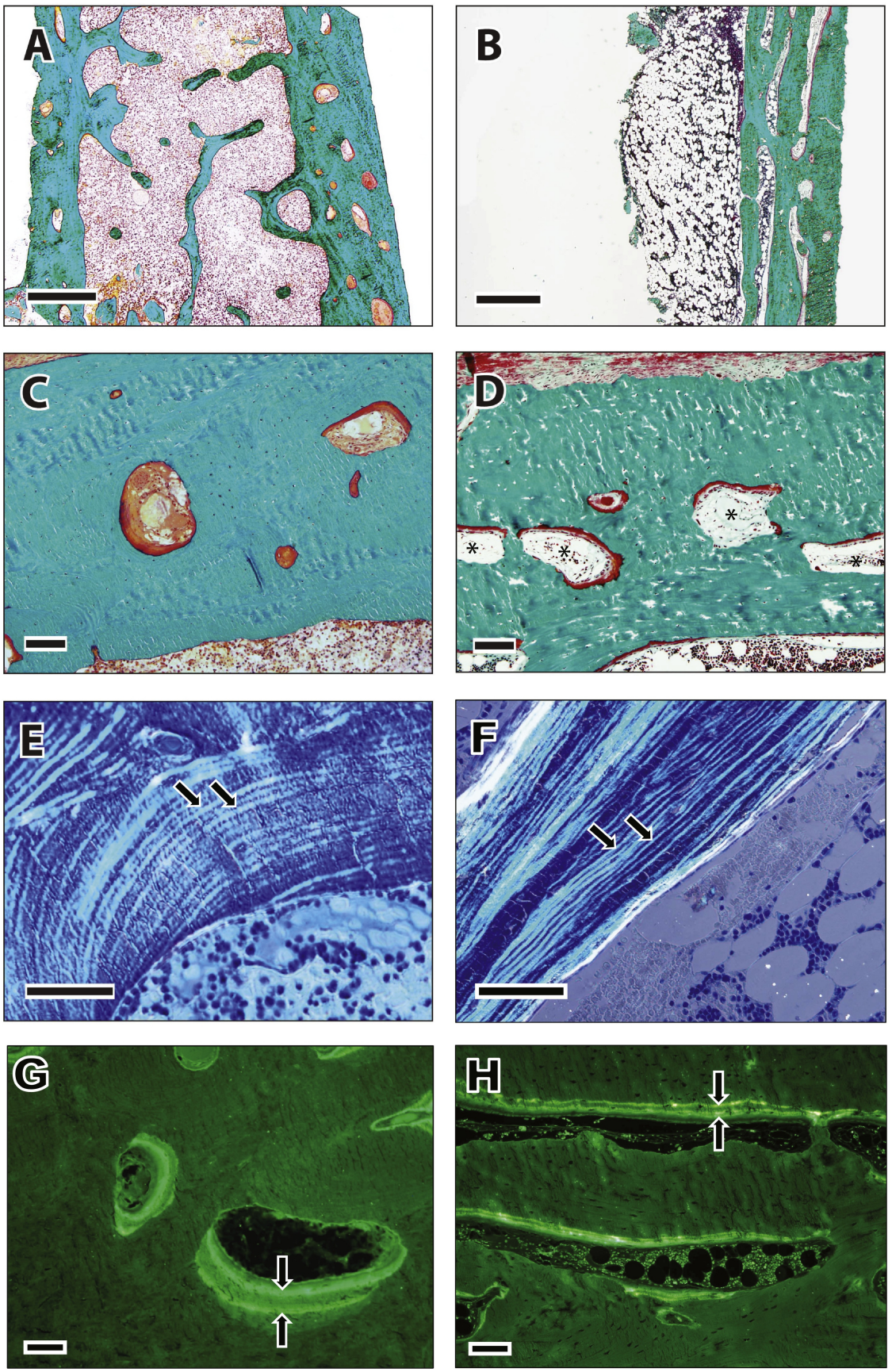

Figure 3